이학석사 학위논문

Impacts of stratospheric ozone on the Southern Hemisphere circulation in the CCMI models

CCMI 모형에서 성층권 오존의 변화가 남반구 순환 변화에 미치는 영향

2020 년 8 월

서울대학교 대학원

협동과정 계산과학

한 보 름

Abstract

We examine the impacts of stratospheric ozone on Southern Hemisphere (SH) zonal mean circulation changes in state-of-the-art chemistry-climate models from Chemistry-Climate Model Initiative (CCMI) project. First, we evaluate total column ozone (TCO) and ozone depletion induced tropospheric circulation changes in the CCMI. Most models successfully reproduce observation and reanalysis data in the late 20th century. Ozone-hole-induced changes are also robust regardless of the specific chemical-atmosphere-ocean coupling. Since greenhouse gases (GHG) also affect SH circulation changes, the relative importance of ozone and GHG are investigated by examining the single forcing experiments from the CCMI. In particular, the fixed ozone-depleting substance (ODS) simulations, and the fixed GHG simulations are directly compared with the reference simulations for both the past and future. Consistent with previous studies, the SH-summer general circulation changes, such as changes in the jet location, Hadley cell edge, and Southern Annular Mode, show opposite trends from the past to the future in response to the Antarctic ozone depletion and recovery. The GHG-induced circulation changes enhance the ozone-induced circulation changes in the past, but partly cancel them in the future. These results suggest that stratospheric ozone is the primary driver of the SH circulation changes in the past. However, both

stratospheric ozone and greenhouse gas are the major factors influencing the SH circulation in the future climate, confirming previous studies.

Keywords: stratospheric ozone, greenhouse gas, Southern Hemisphere, jet location, Hadley cell expansion

Student Number: 2018-20597

Table of Contents

List of tables

List of figures

where surface boundary conditions are prescribed (see table 1).

Figure 7. Temporal evolution of September-November (SON) total column ozone (TCO), integrated poleward of 60°S, from (a) CCMI-C2, (b) ODS and (c) GHG runs.

Figure 8. Multi-model mean (MMM) linear trends of the monthly mean polar (a) ozone [O3] and (b) temperature [T] averaged over 60°-90°S for the period of 1961-2000 in the CCMI-1, CCMI-C2 runs. (c) Same as (a), but for the zonal wind [U] averaged over 65°-55°S. Starting month in the x-axis is July. Statistically significant trends are dotted at the 95% level. (d-f) Same as (a-c) but for the period of 2001-2100.

Figure 9. The MMM long-term mean (thick black contour) and linear trend (shading) of DJF temperature over the period of 1961-2000 for (a) CCMI-C2, (b) ODS, and (c) GHG runs. (d-f) Same as (a-c) but for the zonal wind. Contour intervals are 10 K starting from 200K (Figure 9a-9c) and 10 m s^{-1} starting from 10 m s^{-1} (Figure 9d-9f). Statistically significant trends are dotted at the 95% level.

Figure 10. Same as figure 9 but for the period of 2001-2100.

Figure 11. (a) The ONDJ polar temperature trend at 100 hPa (K /decade) for the period of (left) 1961-2000 and (right) 2001-2100. MMM trends are shown in closed circles with 5-95% confidence levels by a bootstrap method for the additivity (green), CCMI-C2 (black), ODS (red), and GHG (blue) runs. Each model trend is denoted with light colored circles. MMM values become statistically significant when the 5-95% confidence limits do not intersect the zero trend line. (b, c, and d) Same as (a) but for the trends in SAM index (decade^{-1}), Hadley cell edge (degree/decade), and DJF 850-hPa jet location (degree/decade), respectively.

Figure 12. The relationship of DJF jet-latitude trends to DJF Hadley-cell edge trends over the period of 1961-2000 for (a) CCMI-C2, (b) ODS, and (c) GHG runs. (d-f) Same as (a-c) but for the period of 2001-2100. Each model ensemble mean is denoted with open circles. Each ensemble is denoted with a x mark. Correlation coefficient between the two variables is calculated for all model ensemble means and for all ensembles (shown in parenthesis).

1. Introduction

The Southern Hemisphere (SH) circulation has undergone significant changes in the late 20th century. The Southern Annular Mode (SAM), a representative variability of the Southern Hemisphere circulation, has a positive trend, which means that the sea level pressure at high latitudes is relatively lower and at mid-latitudes is higher. It increases the pressure gradient between high latitudes and mid-latitudes (Thompson et al., 2000; Thompson and Solomon, 2002; Marshall, 2003; Fogt et al., 2009). As the pressure gradient strengthened, the tropospheric jet near 60°S was strengthened and shifted toward the Antarctic (Chen and Held, 2007; Previdi and Polvani, 2014; Swart et al., 2015). The storm track, known to be affected by jet, also shifted (Gillett et al., 2006; Archer and Caldeira, 2008) while the Hadley cell expanded, and its edge shifted to the Antarctic (Hu and Fu, 2007; Garfinkel et al., 2015). In response to these changes, the surface climate has changed significantly.

It is well documented that changes in austral summer circulation in the late 20th century are due to ozone depletion (Son et al., 2009; Son et al., 2010; Polvani et al., 2011a). In the 1960s, a decrease in ozone concentration due to increased emissions of ozone-depleting substances

(ODS) created a qualitatively similar pattern to positive SAM. At the same time, the mid-latitude jet shifted towards the South pole, changing the SH circulation (Son et al., 2009). Ozone has been increasing since 2000 as the Montreal Protocol was adopted to reduce ODS. The ozone in the future is expected to continue to increase and return to the 1960 level. Ozone recovery reverses the trends of the past changes in the SH circulation (Perlwitz et al., 2008; Polvani et al., 2011b).

Greenhouse gases, which have continued to increase, are known to change the SH circulation. It increases the temperature of the upper troposphere and increases the temperature gradient between low and high latitudes. As a result, the tropospheric jet is strengthened and shifts toward the Antarctic. Previous studies compared the effects of ozone and greenhouse gases, two factors affecting the Southern Hemisphere circulation, to find a dominant driver (Mclanderess et al., 2011; Polvani et al., 2011b). In the past, the Southern Hemisphere circulation was dominant due to ozone depletion (Polvani et al., 2011a). In the future, there was a weaker intensity change than in the past by canceling the effect of ozone recovery and increasing greenhouse gases. In this study, we focused on the methods from the multi-model analysis conducted in the previous studies and applied them to the latest atmospheric chemistry model, CCMI.

2. Data and Methodology

The CCMI project, initiated by the International Global Atmospheric Chemistry (IGAC) and the Stratosphere-troposphere Processes And their Role in Climate (SPARC), includes a state-of-the-art chemistry-climate interactions model. This project is an extension of the CCMVal2 (Eyring et al., 2010), but differs in that CCMVal2 models are interactive only in stratospheric chemistry (Morgenstern et al., 2010). CCMI models are fully interactive not only in stratospheric chemistry but also in tropospheric chemistry (Table 1). As listed in Table 1, 15 CCMI models are used in this study.

Among the simulations provided by CCMI, four simulations were used for this analysis: REF-C1, REF-C2, SEN-C2-fGHG, and SEN-C2-fODS. The REF-C1 (hereafter CCMI-C1) experiment is a historical simulation performed from 1960 to 2010 prescribing surface boundary conditions with observations. REF-C2 (hereafter CCMI-C2) experiment, spanning the period 1960-2100, is conducted with coupled ocean or modeled surface boundary conditions. It is noted in table 1 which of the models have ocean coupling. These models allow us to evaluate the role of atmosphere-ocean coupling in the SH climate change. This experiment uses the A1 scenario of WMO (2011) for ODSs, which is almost identical

to the scenario used by CCMVal-2 (SPARC, 2010). Other greenhouse gases (GHGs), tropospheric ozone, and aerosols develop according to historical values and RCP 6.0 (Meinshausen et al., 2011). Two sensitivity simulations are further examined. SEN-C2-fODS (hereafter GHG) is the same as CCMI-C2 but with ODSs fixed at their 1960 levels. Sea surface and sea ice conditions in this simulation are prescribed as the 1955-1964 average. SEN-C2-fGHG (hereafter ODS) is the same as CCMI-C2 but with GHGs fixed at their 1960 levels. Comparing these two experiments allows us to quantify the relative effects of ODSs and GHGs on SH general circulation changes, respectively.

Model datasets are interpolated into a uniform 2.5° × 2.5° grid with 31 vertical levels. In section 3.1, CCMI-C1, a simulation of the past period, was used to confirm that the simulated ozone is similar to the observation using monthly total column ozone (TCO) data. In section 3.2, CCMI-C1 and CCMI-C2 simulations were used to compare the effect of surface boundary conditions in the SH circulation. The monthly zonal wind, TCO, varying vertical ozone, and temperature data are used. In section 3.3, CCMI-C2, GHG, and ODS simulations were used to compare which changes in the Southern Hemisphere circulation were caused by ozone depletion and greenhouse gas increase. The variables used are monthly zonal wind, meridional wind, ozone, temperature, and geopotential height.

CMIP5 is used for comparison with CCMI to identify the importance of interactive chemistry in section 3.2. In this study, only the high-top models with a model top at 1 hPa or higher are considered (Table 2). Most CMIP5 models are forced by the SPARC ozone data or its modified version (Eyring et al., 2013). However, several models have fully interactive ozone chemistry and are qualified as CCMs (four models in Table 2). The monthly zonal wind is used for this study.

Most of the analysis in this study is based on the multi-model mean (MMM) and the linear trends by a least-square fitting. MMM is performed from each model's ensemble mean rather than all individual ensemble members. This approach reduced an overweighting the models with a large number of ensemble members. The several indices quantify the SH general circulation changes as in Son et al. (2010) for section 3.3. Stratospheric temperature was calculated by averaging 100 hPa temperature for the zonal and 60-90° S. Hadley Cell (HC) edge was defined as the zero-crossing latitude of 500 hPa mass stream function in the SH subtropics. The jet location was determined as the latitude where an 850 hPa zonal-mean zonal wind has the maximum. We applied the common basic function approach (e.g., Lee et al. 2019) to calculate the SAM index since each model reproduces the leading pattern differently. The first leading mode was obtained by the empirical orthogonal

function using the JRA-55's 850 hPa geopotential height. We project each model data into the first leading mode for the time series.

3. Results

3.1 Evaluation of total column ozone in CCMI models

The CCMI models and observation data are compared to evaluate that the CCMI models reproduced observation well. The analysis period is 1979-2010 (32 years), in which observation data was available, and CCMI-C1 simulations are used. Figure 1 shows the spatial distribution of the annual mean of TCO. According to observations, the Northern Hemisphere showed the most substantial TCO concentration in the Sakhalin of northern Japan and the Kamchatka Peninsula. This large amount of TCO is due to ozone coming down from the tropopause of this region, where the wave breaking is active (Hipskind, 1987; 이혜란, 1999). In the Southern Hemisphere, TCO is high at around 60°S in southwest Australia. Low latitudes and the Antarctic show relatively low TCO. The spatial distribution of the TCO is well reproduced in most CCMI models compared to observations. Although there are differences in the values, there is high concentration TCO in the high latitude of the Northern Hemisphere and a low concentration in the equatorial and Antarctic regions. Out of CCMI modes, UMUKCA-UCAM underestimated TCO in Southern Hemisphere. Figure 2 displays the Taylor diagram of the spatial distribution of the annual mean TCO. This figure shows the

pattern correlation and normalized standard deviation comparing each model with the observation. Each CCMI model is circled in the same color as the legend, and observation is shown in circle colored in black. All CCMI models show spatial distribution similar to observation, with a pattern correlation of 0.9 or higher. The normalized standard deviations show the variation of spatial distribution between model and observation. It can be seen that all models show little differences in variation of observation. Most models well reproduce the phase and amplitude of observed annual cycle of TCO and the spatial distribution of TCO trends (not shown).

3.2 Impacts of ozone depletion on Southern Hemisphere circulation changes and effects of interactive ocean

In section 3.1, we confirmed that the CCMI models simulated ozone similarly to observations. In section 3.2, changes in the SH circulation from 1960 to 2000, when ozone depletion was observed, are examined using CCMI and CMIP5 models.

Figure 3 presents the temporal evolution of September-November (SON) TCO anomaly, integrated poleward of 60°S with area weight, for each model. Here, an anomaly is defined as the deviation from the 1980-2000 climatology of each model. All models, i.e., CCMI-CI, CCMI-C2, and

CMIP5 models, successfully reproduce the observed ozone depletion. This is especially true in the 1980s and 1990s when the simulated TCO trends are quantitatively similar to those derived from the two satellite products (Bodeker et al., 2005; Van der A et al., 2015). The spatial distribution of monthly-mean TCO and its seasonal cycle are also reasonably well captured (not shown). A comparison between figure 1a and 1b further reveals that for each given model, the CCMI-C1 and CCMI-C2 simulations have a quantitatively similar TCO evolution (compare the same color on each panel). Since the two experiments differ only in their surface boundary conditions, this result may suggest that stratospheric ozone chemistry and transport is only weakly sensitive to the details of surface boundary conditions.

A pronounced inter-model spread, however, is evident in the 1960s and 1970s (Figures 3a and 3b). This divergence among the models is similar to that seen in the CCMVal2 models (Austin et al., 2010) and indicates that CCMs still have significant uncertainty in ozone simulation. The inter-model spread becomes much larger if TCO, instead of its anomaly, is considered (not shown). Unlike the CCMI models, the CMIP5 models show a quantitatively similar TCO evolution (figure 3c). This is anticipated because most CMIP5 models are forced by the SPARC ozone data or its modified version. The CMIP5 models with interactive ozone chemistry also show a similar TCO evolution (see the dashed lines in

figure 3c).

The vertical structure of polar ozone trends is further illustrated in the first column of figure 4. The ozone depletion in the CCMI simulations is maximum at ~ 50 hPa in October. This is quantitatively similar to the one derived from the SPARC ozone data (e.g., figure 4c). The subtle differences among the experiments, such as a slightly stronger ozone depletion in CCMI-C2 runs than in CCMI-C1 runs and a stronger upper-stratospheric ozone depletion in CCMI runs than in CMIP5 runs, are mostly insignificant.

The temperature response to the ozone depletion and the related stratospheric change is presented in the middle column of figure 4. All experiments show significant cooling centered at ~70 hPa in November. This cooling trend is extended from the upper stratosphere to the lower stratosphere with a maximum cooling at 20 hPa in October but at 200 hPa in December. Due to the thermal wind balance, a strong cooling in late spring is accompanied by a strengthening of the polar vortex (third column of figure 4). This acceleration, which is maximum in November, is not confined within the stratosphere but is extended to the troposphere. A statistically significant tropospheric trend is particularly evident in December.

The temporal and vertical structure of polar ozone, temperature

and mid-latitude wind trend (figure 4) is remarkably similar to that of the CCMVal2 simulations. This may suggest no major differences in multi-model mean trends between the CCMVal2 models and their updated versions. The similarity between the experiments is further confirmed by the latitudinal structure of December-February (DJF) zonal-mean zonal wind trend (figures 5b-d). For reference, the trend derived from the Japanese 55-year Reanalysis (JRA-55; Ebita et al, 2011) is also displayed in figure 5a (this data is chosen simply because it is the latest reanalysis dataset covering the whole analysis period). All experiments show quantitatively similar poleward intensification of westerly jet that resembles the reanalysis trend and the CMIP3/CCMVal2 trends (e.g., figure 4 of Gerber et al. 2012). The CMIP5 models show a somewhat weaker polar vortex change compared with the CCMI models (figure 5d). This underestimation is mainly due to the models with a prescribed ozone depletion (figure 5f). The models with interactive chemistry (four models listed in Table 2) show essentially the same jet trend to the CCMI models (figure 6). However, regardless of polar vortex changes, the CMIP5 models show quantitatively similar tropospheric circulation change. This result is consistent with Eyring et al. (2013) who documented that the CMIP5 models with interactive chemistry have a larger inter-model spread and are not well separated from those without interactive chemistry (see their figures 10 and 11).

These results clearly suggest that the ozone-hole-induced tropospheric change is not strongly sensitive to the details of surface boundary conditions (prescribed versus coupled ocean) and ozone forcing (prescribed versus interactive ozone) when the multi-model mean trends are considered. This conclusion is accentuated by the latitudinal distribution of 850-hPa zonal wind trend which is almost identical among the model ensembles (figure 6). All experiments show quantitatively similar multi-model mean trends. In figure 3f, the CCMI models with and without a coupled ocean are separately compared (solid lines). Likewise, the CCMI models with observed and modeled surface boundary conditions are compared (dashed lines). Again, each group shows the same multi-model mean trend, confirming the above conclusion.

3.3 Comparison of the impact of stratospheric ozone and greenhouse gases on Southern hemisphere circulation changes

In section 3.2, we identified that Southern Hemisphere circulation changed in CCMI models when ozone decreases dramatically from 1960 to 2000. The simulations used in the previous section, however, include not only the effects of stratospheric ozone but also the effects of

greenhouse gases. Although previous studies show that ozone depletion is a significant driver of Southern Hemisphere circulation change in the late 20C, quantifying the relative importance between ozone and greenhouse gases is needed. We examined historical and projected future circulation using simulations with single-forcing experiments, which are fixed ozone depletion substances (GHG runs) and fixed greenhouse gases (ODS runs).

Figure 7 presents the time series of SON TCO, integrated poleward from 60° S, from 1960 to 2100 for each model and multi-model mean (MMM). CCSRNIES-MIROC3.2 (orange line) simulates lower TCO than the other 5 models in all simulations, e. g., CCMI-C2, ODS, and GHG. CHASER-MIROC-ESM (light green) shows ozone recovery earlier than other models in ODS simulation. MMM trend changed as of 2000 in CCMI-C2 and ODS simulations. From 1960 to 2000, CCMI models well reproduced ozone depletion caused by increasing ozone depletion substances (ODSs). In 2100, CCMI models project TCO recovery at the 1960's level in CCMI-C2 and ODS runs. TCO does not show the significant trend in the GHG experiments because of ODSs fixed at 1960 levels throughout the experiments. Therefore, in section 3.3, the period was divided into two periods from 1960 to 2000, when ozone decreases until 2000, and from 2001 to 2100, when ozone gradually recovers to

the 1960s level. Figure 8 shows monthly-mean trends in CCMI-2 simulation. The vertical structure of polar ozone, temperature, and mid-latitude wind trends of CCMI models remarkably resemble that of CCMVal-2 simulations (Son et al., 2010). Similar to figure 4, ozone depletion causes radiative cooling in the lower stratosphere (figure 8a, 8b). The temperature gradient between low and high latitudes accelerates the zonal wind trend in the past (figure 8c). Figures 8d-8f show future trends in CCMI-C2 simulation. The future trends of CCMI in the stratosphere show the qualitatively similar structure with an opposite sign as that of the past. The response of lower troposphere mid-latitude jet, however, is not completely opposite compared to the past. Unlike the past, zonal wind changes are not linked to the troposphere, and weak tropospheric acceleration is shown in the future. It might be due to O_3 and GHGs playing an opposite role in the SH circulation changes in the future.

Figure 9 shows the trends in DJF zonal-mean temperature and zonal wind in each run (shading) with their climatology (contour) for 1961-2000. In the past, CCMI-C2 and ODS runs are quite similar. Temperature trends of the polar cap are decreased by ozone depletion. The tropical upper-tropospheric warming trends emerge in GHG runs. Westerlies trends in upper troposphere-lower stratosphere (UTLS) regions increase at 60°S in CCMI-C2 and ODS runs. The intensified westerlies propagate downward to

the surface. It accompanied with a poleward shift of mid-latitude jet. In GHG runs, a weak acceleration is observed in the extratropics and mid-latitude jet does not show a significant poleward shift. CCMI models confirm that DJF circulation changes in the Southern Hemisphere are mainly driven by ozone depletion in the past. Figure 10 shows Southern Hemisphere circulation in 2001-2100 when ozone recovers in CCMI-2 and ODS run. Ozone recovery induces radiative warming of polar lower stratospheric temperature in CCMI-C2 and ODS runs (Figures. 10a and 10b). Continuous increase of greenhouse gases induce warming of the upper troposphere in the tropics in the CCMI-C2 and GHG runs (Figures. 10a and 10c). Opposite zonal wind trends of comparable magnitude are found in ODS (Figure. 10e) and GHG (Figure. 10f) runs. ODS- and GHG-induced troposphere jet are opposite to each other. In the past, the magnitudes of ODS-induced climate change are larger than GHG-induced changes. In the future, however, ODS-and GHG-induced changes are comparable.

The MMM trends (dark color) and inter-model spread (light color) of circulation changes in the Southern Hemisphere are quantified for the periods 1961-2000 (left) and 2001-2100 (right) (Figure. 11). Green, black, red, and blue marks denote the additivity, CCMI-C2, ODS, and GHG runs, respectively. Figure 11a shows the polar cap temperature trends in the late spring-early summer (October-to-January; ONDJ) at 100 hPa. The ODS runs of CCMI models show significant cooling in the past, its magnitude is

comparable to that in CCMI-C2. In the future, ODS and CCMI-C2 runs show significant warming trend. The temperature trends in GHG runs in the past are negligible, however, a weak negative trend is found in the future. Ozone depletion and has strengthened the dipolar change of sea level pressure. Ozone recovery has weakened that change (Figure 11b). Increasing greenhouse gases show positive trend of SAM index in the future. DJF Hadley cell edge and DJF jet shifted poleward in ozone depletion. Ozone recovery tends to shift the Hadley cell and jet equatorward in DJF. The additivity (green) magnitude is comparable to that in CCMI-C2 except for the DJF SAM index in 1961-2000. This implies that ODS and GHG explain most of the CCMI-C2 run than other anthropogenic forcings. Those trends are predicted to be weakened and the inter-model spread is smaller in the future than in the past. For inter-model spread, the polar cap temperature trends show a smaller intensity compared to those in the changes in SAM index, Hadley cell edge, and location of the extratropical jet.

Figure 12 displays the relationship between trends of DJF Hadley cell edge and trends of DJF jet latitude in the past (top) and future (bottom). Correlations between all models are 0.87, 0.82, and 0.94 in CCMI-C2, ODS, and GHG runs, respectively. Correlations in GHG runs are higher than CCMI-C2 and ODS runs for all models and ensemble. CMAM overestimated Hadley cell edge change and jet latitude in CCMI-C2 and GHG runs in the past. Consistent with figure 11, the inter-model spread is

small in the future. Correlation in the future is higher than in the past for ODS runs.

4. Summary and Conclusions

We evaluate that CCMI models, state-of-the-art CCMs, reasonably well reproduce TCO. Most CCMI models show qualitatively similar spatial distribution of TCO to observation, and quantitatively, the correlation with observation are very high, over 0.9. CCMI models show similar time evolution of TCO and trends to observation in austral spring. The circulation changes of the SH due to ozone depletion are also similar to the reanalysis data. Decreasing of lower stratospheric temperature induce temperature gradient between high and low latitude. Due to the thermal wind balance, the jet is intensified. Jet intensification is linked from the stratosphere to the troposphere. CCMI-C1 and CCMI-C2 runs with different sea surface temperature and sea ice concentration show qualitatively similar MMM trends. CCMI with interactive chemistry and CMIP5 with prescribed ozone also exhibit similar jet trends. Boundary condition and interactive chemistry are not sensitive Southern Hemisphere circulation compared inter-model spread.

In the CCMI-C1 and CCMI-C2 simulations, not only the effects of ozone depletion but also the forcing of greenhouse gases and aerosols are included. To quantify relative importance, we re-examine the stratospheric ozone and GHG impacts in CCMI models on the SH zonal-

mean circulation changes using single forcing experiments. The multi-model mean and inter-model spread of 6 models are evaluated for the past (1961-2000) and future (2001-2100). In the past, ozone depletion is the main driver of Southern Hemisphere circulation changes. CCMI-C2 and ODS simulations show poleward expansion of the Hadley cell and a poleward shift of the westerly jet accompanied by the positive trends in the SAM index. The impacts of GHGs are different for each model and the inter-model spread is large. In the future, as ozone recovers, it affects the Southern Hemisphere circulation as opposed to the past. It was confirmed that the intensity of the future changes is weak by canceling the effect of ozone and greenhouse gases.

Although the ozone-depleting substances around the world are decreasing due to the Montreal Protocol, however, it has recently been reported that CFC emissions have increased. This has slowed ozone recovery. In the model scenario, this issue is not updated. Further studies and model experiments should be considered under the new conditions.

Acknowledgement

The present study is originated in part from Son et al., 2018: Tropospheric jet response to Antarctic ozone depletion: An update with Chemistry-Climate Model Initiative (CCMI) models. *Environmental Research Letters*, **13**, 054024.

5. References

이혜란. 1999: 오존 전량의 시, 공간 변동 및 대기 열적 상태와의 상관. 석사학위논문, 이화여자대학교 교육대학원, 서울.

Archer, C., and K. Caldeira, 2008: Historical trends in the jet streams. *Geophysical Research Letter*, **35**, L08803.

Austin, J. et al., 2010: Decline and recovery of total column ozone using a multimodel time series analysis. *J. Geophys. Res. Atmos.* **115**, D00M10.

Bodeker, G. E., H. Shiona, and H. Eskes, 2005: Indicators of Antarctic ozone depletion. *Atmospheric Chemistry and Physics,* **5**, 2603-15.

Chen, G., and Held, I. M. 2007: Phase speed spectra and the recent poleward shift of Southern Hemisphere surface westerlies. *Geophysical Research Letters*, **34**.

Ebita, A. et al. 2011: The Japanese 55 year reanalysis 'JRA-55': an interim report. *SOLA*. **7**, 149-52.

Eyring, V., Shepherd T. G., and Waugh, D. W., 2010: Chemistry climate model validation. *SPARC Rep.* **5**, 426.

---, V. et al. 2013: Long-term ozone changes and associated climate impacts in CMIP5 simulations. *J. Geophys. Res. Atmos.* **118**, 5029-60

Fogt, R. L., Perlwitz, J., Monaghan, A. J., Bromwich, D. H., Jones, J. M., and Marshall, G. J., 2009: Historical SAM variability. Part II: Twentieth-century variability and trends from reconstructions, observations, and the IPCC AR4 models. *Journal of Climate*, **22**, 5346-5365.

Garfinkel, C. I., Waugh, D. W., and Polvani, L. M., 2015: Recent Hadley cell expansion: The role of internal atmospheric variability in reconciling modeled and observed trends. *Geophysical Research Letters*, **42**, 10-824.

Gerber, E. P. et al., 2012: Assessing and understanding the impact of stratospheric dynamics and variability on the Earth system. *Bull. Am. Meteor. Soc.* **93**, 845-59.

Gillett, N. P., Kell, T. D., and Jones, P. D, 2006: Regional climate impacts of the Southern Annular Mode. *Geophysical Research Letters*, **33**, L23704.

Hipskind, R. S., Gregory, G. L., Sachse, G. W., Hill, G. F., and Danielsen, E. F. 1987: Correlations between ozone and carbon monoxide in the lower stratosphere, folded tropopause, and maritime troposphere. *Journal of Geophysical Research: Atmospheres*, **92**, 2121–2130.

Hu, Y., and Fu, Q., 2007: Observed poleward expansion of the Hadley circulation since 1979. *Atmospheric Chemistry and Physics,* **7**, 5229–36.

Lee, D. Y., Petersen, M. R., and Lin, W., 2019: The southern annular mode and southern ocean surface westerly winds in E3SM. *Earth and Space Science*, **6**, 2624–2643.

Marshall, G. J., 2003: Trends in the Southern Annular Mode from observations and reanalyses. *Journal of climate*, **16**, 4134–4143.

McLandress, C., Shepherd, T. G., Scinocca, J. F., Plummer, D. A., Sigmond, M., Jonsson, A. I., and Reader, M. C., 2011: Separating the dynamical effects of climate change and ozone depletion. Part II: Southern Hemisphere troposphere. *Journal of Climate*, **24**, 1850–1868.

Meinshausen, M. et al., 2011: The RCP greenhouse gas concentrations and their extensions from 1765 to 2300, *Clim. Change*, **109**, 213–241.

Morgenstern, O. et al., 2010: Review of the formulation of present–generation stratospheric chemistry–climate models and associated external forcings. *J. Geophys. Res. Atmos.* **115**, D00M02.

———, O. et al., 2017: Review of the global models used within phase 1 of the Chemistry–Climate Model Initiative (CCMI). *Geoscientific Model Development*, European Geosciences Union, 2017, **10**, 639 – 671.

Perlwitz, J., Pawson, S., Fogt, R. L., Nielsen, J. E., and Neff, W. D., 2008: Impact of stratospheric ozone hole recovery on

Antarctic climate. *Geophysical Research Letters*, **35**, L08714.

---, M., and Polvani, L. M., 2014: Climate system response to stratospheric ozone depletion and recovery. *Quarterly Journal of the Royal Meteorological Society*, **140**, 2401-2419.

Polvani, L. M., Waugh, D. W., Correa, G. J., and Son, S. W., 2011a: Stratospheric ozone depletion: The main driver of twentieth-century atmospheric circulation changes in the Southern Hemisphere. *Journal of Climate*, **24**, 795-812.

---, L. M., Previdi, M., and Deser, C., 2011b: Large cancellation, due to ozone recovery, of future Southern Hemisphere atmospheric circulation trends. *Geophysical Research Letters*, 38.

---, S. W., Tandon, N. F., Polvani, L. M., and Waugh, D. W., 2009: Ozone hole and Southern Hemisphere climate change. *Geophysical Research Letters*, **36**, L15705.

---, S. W. et al., 2010: Impact of stratospheric ozone on Southern Hemisphere circulation change: A multimodel assessment. *Journal of Geophysical Research: Atmospheres*, **115,** D00M07.

SPARC, 2010: SPARC CCMVal Report on the Evaluation of Chemistry-Climate Models, edited by: Eyring, V., Shepherd, T. G., and Waugh, D. W., *SPARC Report No. 5*, WCRP-30/2010, WMO/TD - No. 40.

Swart, N. C., Fyfe, J. C., Gillett, N., and Marshall, G. J., 2015: Comparing trends in the southern annular mode and surface westerly jet. *Journal of Climate*, **28**, 8840-8859.
1018 - 1036

Thompson, D. W., and Wallace, J. M., 2000: Annular modes in the extratropical circulation. Part I: Month-to-month variability. *Journal of climate*, **13**, 1000-1016.

---, and Solomon, S., 2002: Interpretation of recent Southern Hemisphere climate change. *Science*, **296**, 895-899.

Van der A, R. J., M. A. F. Allaart and H. J. Eskes, 2015: Extended and refined multi sensor reanalysis of total ozone for the period 1970-2012. *Atmospheric Measurement Techniques,* **8**, 3021-

35.

World Meteorological Organization (WMO), 2011: Scientific assessment of ozone depletion: 2010, *Global Ozone Res. Monit. Proj. Rep.* **52**, 516.

6. Tables

Table 1. List of the CCMI models used in this study. Each model's acronym can be found in Morgenstern et al (2017). The model resolution is indicated in terms of horizontal resolution and the number of vertical levels. The CCMs with only stratospheric chemistry are denoted with "Strat", while those incorporating both stratospheric and tropospheric chemistry are denoted with "Strat-Trop". The models with relatively simple tropospheric chemistry are separately denoted with "Strat-sTrop". The "Coupled" in the fourth column indicates the model in which the ocean is coupled in the CCMI-C2 experiment.

Model	Resolution	Chemistry	CCMI-C2 ocean
ACCESS-CCM	3.75°x2.5° L60	Strat-Trop	Uncoupled
CCSRNIES-MIROC3.2	T42 L34	Strat	Uncoupled
CESM1-CAM4Chem	1.9°x2.5° L26	Strat-Trop	Coupled
CESM1-WACCM	1.9°x2.5° L66	Strat-Trop	Coupled
CMAM	T47 L71	Strat-Trop	Uncoupled
CNRM-CM5.3	T63 L60	Strat	Uncoupled
EMAC-L47MA	T42 L47	Strat-Trop	Coupled
EMAC-L90MA	T42 L90	Strat-Trop	Uncoupled
GEOSCCM	2°x2° L72	Strat-Trop	Uncoupled
HadGEM3-ES	1.875°x1.25° L85	Strat-Trop	Coupled
MRI-ESM1r1	T_L159 L80	Strat-Trop	Coupled
NIWA-UKCA	3.75°x2.5° L60	Strat-Trop	Coupled
SOCOL3	T42 L39	Strat-sTrop	Uncoupled
UMSLIMCAT	3.75°x2.5° L64	Strat	Uncoupled
UMUKCA-UCAM	N48 L60	Strat-sTrop	Uncoupled

Table 2. List of the CMIP5 models used in this study. Only high-top models, that have a model top at 1 hPa and higher, are used. The models with the prescribed ozone are denoted with "Prescribed", while the models with semi-offline chemistry or fully interactive ozone chemistry are denoted with "Semi-offline" or "Strat-Trop", respectively. Note that, unlike the CCMI models, all CMIP5 models are coupled with the ocean.

Model	Resolution	Chemistry
CESM1-WACCM	1.9°x2.5° L66	Strat-Trop
CMCC-CMS	T63 L95	Prescribed
GFDL-CM3	C48 L48	Strat-Trop
HadGEM2-CC	N96 L38	Prescribed
IPSL-CM5A-LR	1.875°x3.75° L39	Semi-Offline
IPSL-CM5A-MR	1.25°x2.5° L39	Semi-Offline
IPSL-CM5B-LR	1.875°x3.75° L39	Semi-Offline
MIROC4h	T213, L56	Prescribed
MIROC-ESM	T42 L80	Prescribed
MIROC-ESM-CHEM	T42 L80	Strat-Trop
MPI-ESM-LR	T63 L47	Prescribed
MPI-ESM-MR	T63 L95	Prescribed
MPI-ESM-P	T63 L47	Prescribed
MRI-CGCM3	T159 L48	Prescribed
MRI-ESM1	T_L159 L48	Strat-Trop

7. Figures

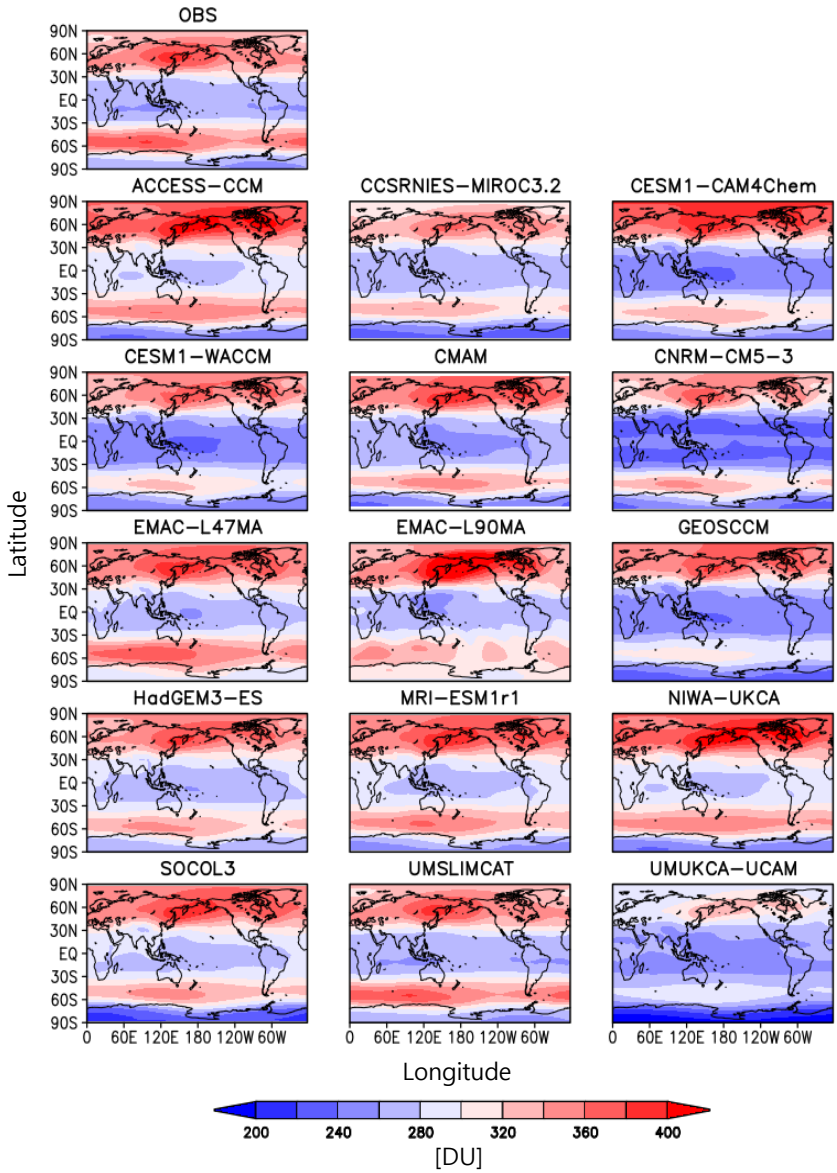

Figure 1. Annual mean total column ozone averaged between 1979-2010 from CCMI models and NIWA-BS observation.

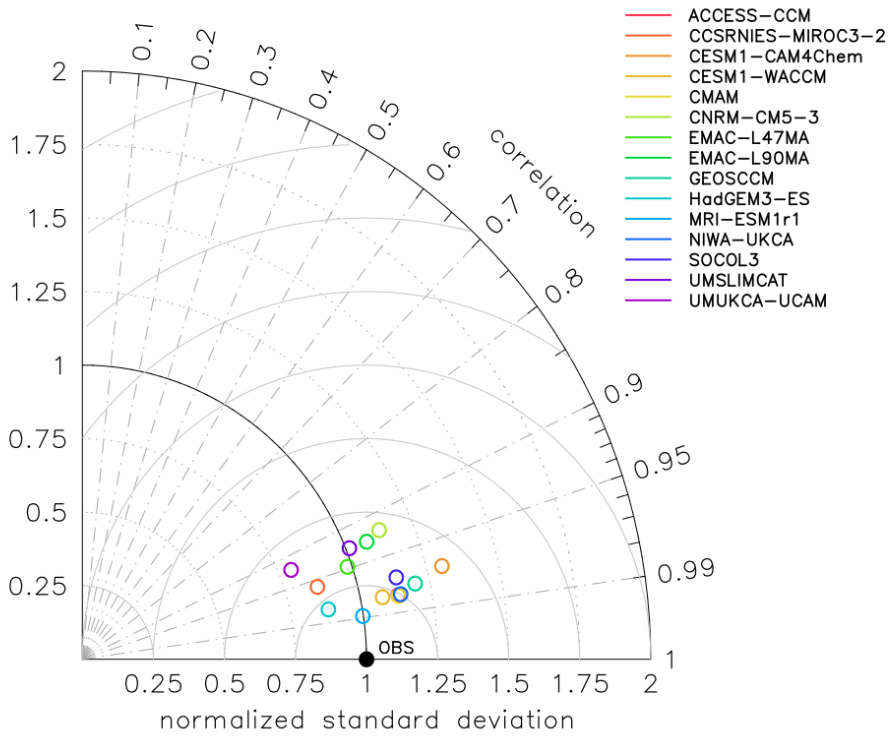

Figure 2. Normalized taylor diagram of annual mean TCO in CCMI models for global spatial pattern.

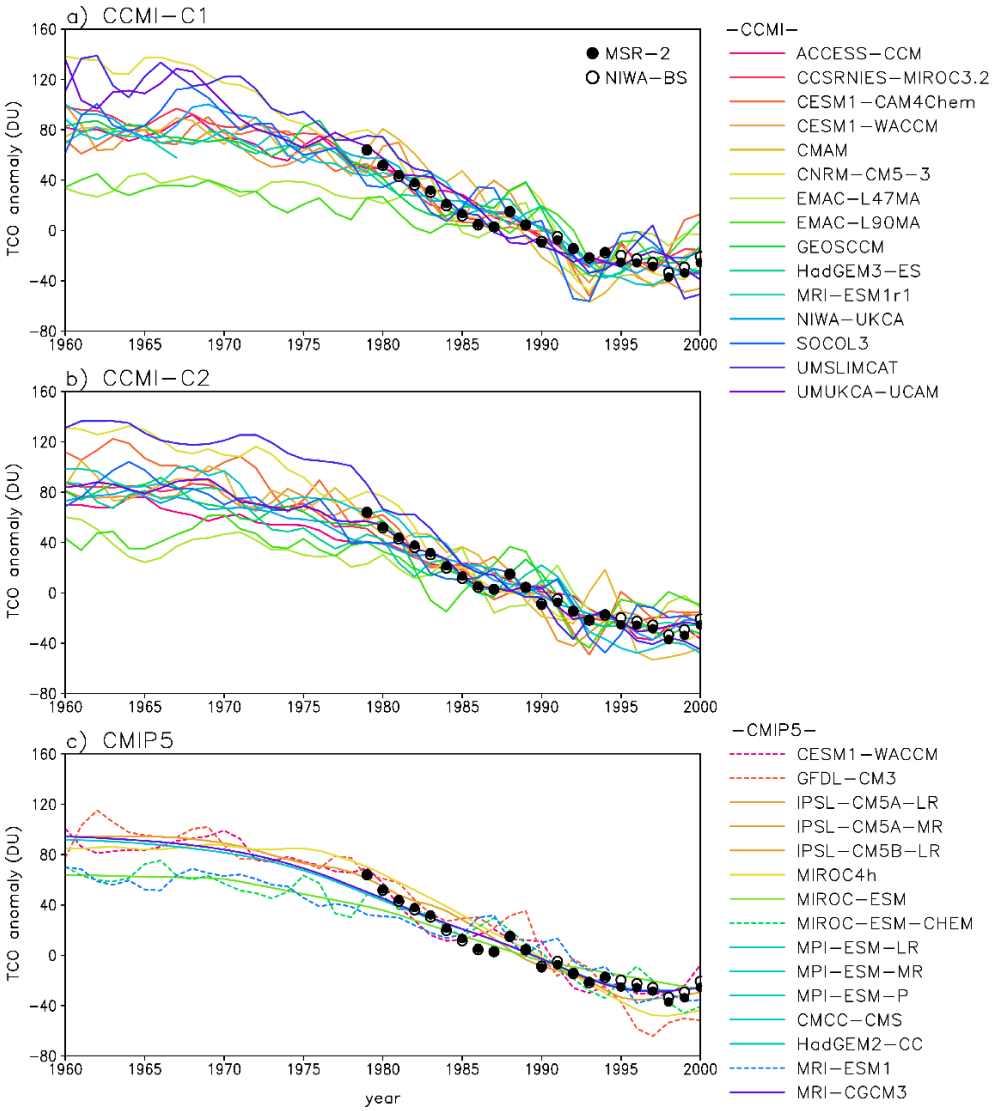

Figure 3. Temporal evolution of September-November (SON) total column ozone (TCO) anomalies, integrated poleward of 60°S, from (a) CCMI-C1, (b) CCMI-C2 and (c) CMIP5 historical runs. The anomaly is defined as the deviation from the 1980-2000 climatology of each model, and is slightly smoothed with a 1-2-1 filter. In (c), TCO anomalies of the models with interactive chemistry are denoted with dashed lines. The models that use the same ozone data (e.g., three MPI-ESM models, CMCC-CMS, and HadGEM2-CC as discussed in Eyring et al 2013) are indicated with the same color. For CCMI reference, the observed TCO anomalies, derived from the MSR-2 and NIWA-BS data sets, are superimposed with filled and open dots, respectively.

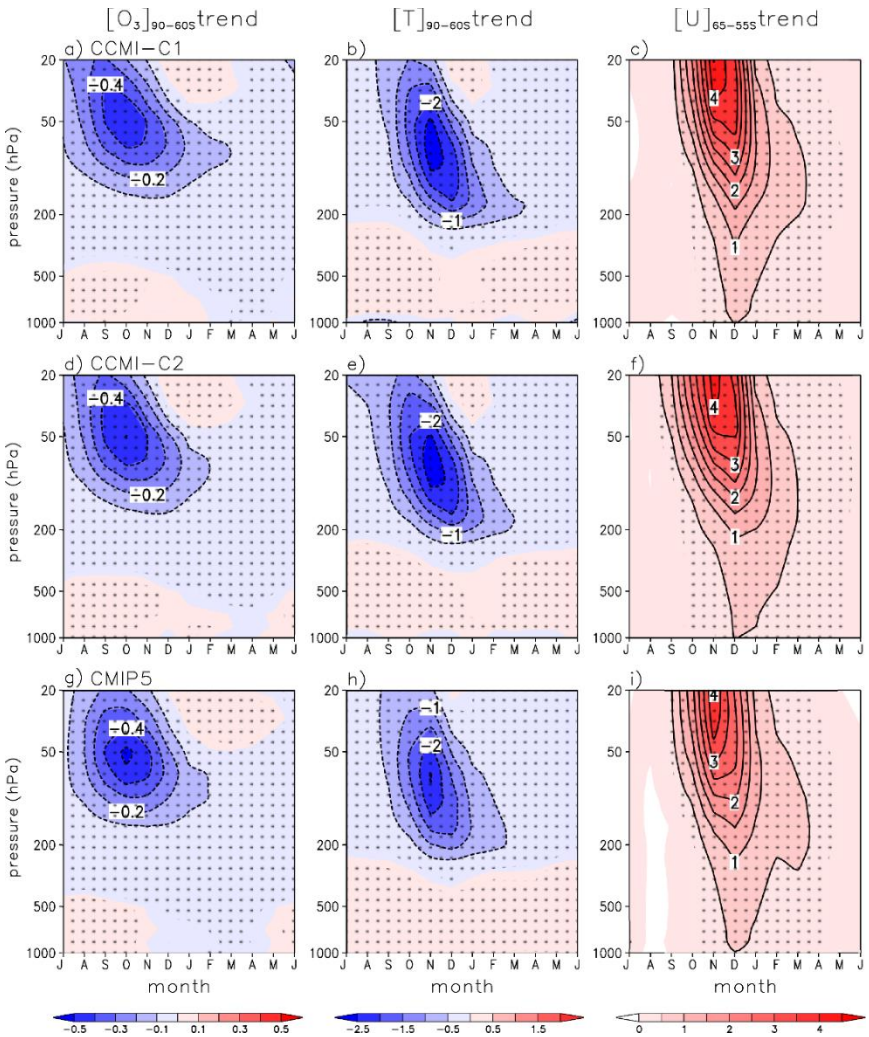

Figure 4. The Multi-model mean trends of (left) monthly-mean polar-cap ozone concentration, (middle) temperature, and (right) mid-latitude zonal wind for the period of 1960-2000 for (top) CCMI-C1, (middle) CCMI-C2, and (bottom) CMIP5 historical runs. Both ozone and temperature are integrated poleward of 60°S with area weight, whereas zonal wind is averaged from 65°S to 55°S. In all panels, x-axis starts from July and ends in June. The contour intervals are 0.1 ppmv/decade for ozone, 0.5 K/decade for temperature, and 0.5 m s^{-1}/decade for zonal wind. The multi-model mean trends that are statistically significant at the 95% confidence level are dotted.

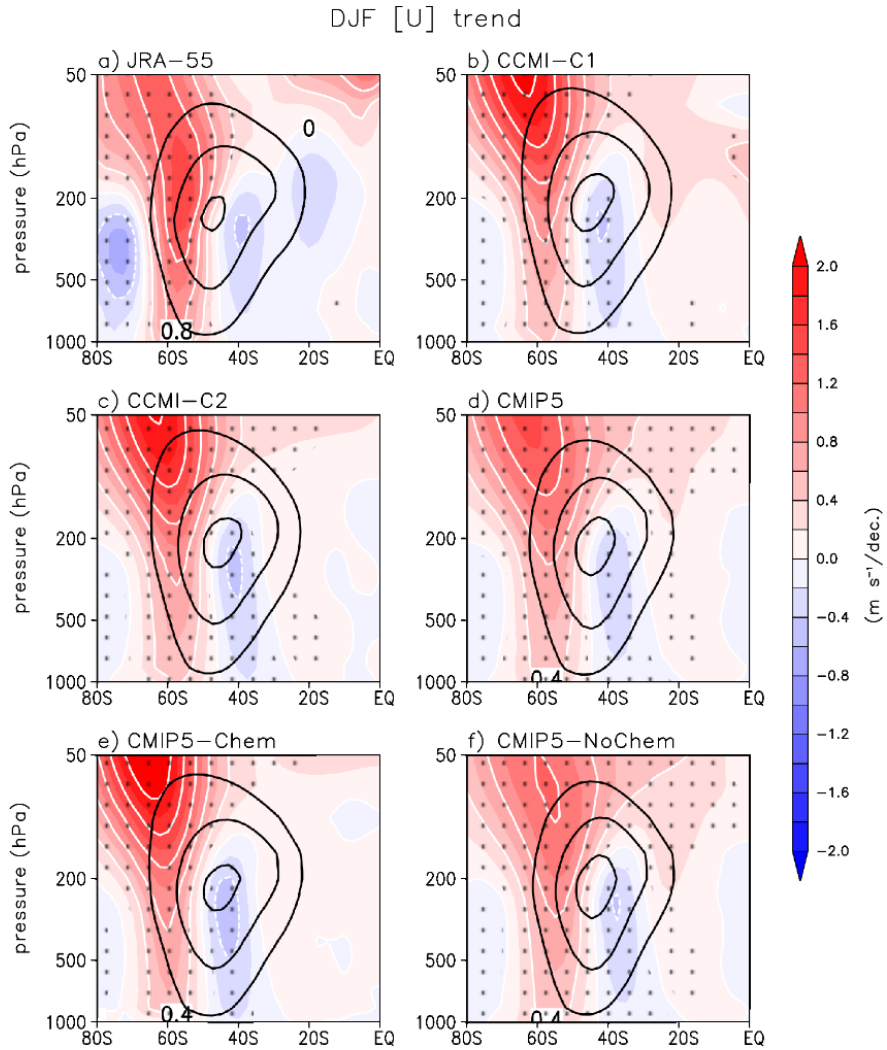

Figure 5. The DJF zonal-mean zonal wind climatology (contour) and long-term trend over 1960-2000 (shading) for (a) JRA-55, (b) CCMI-CI, (c) CCMI-C2, and (d) CMIP5 multi-model means. Contour interval of climatological wind is 10 m s^{-1} starting from 10 m s^{-1}. The trends that are statistically significant at the 95% confidence level are dotted. Bottom panels show (e) 850-hPa zonal wind trends from JRA-55 and model output and (f) sub-composite for the six CCMI-C2 models in which ocean is coupled and the nine models where surface boundary conditions are prescribed (see Table 1 for the list of models for each group).

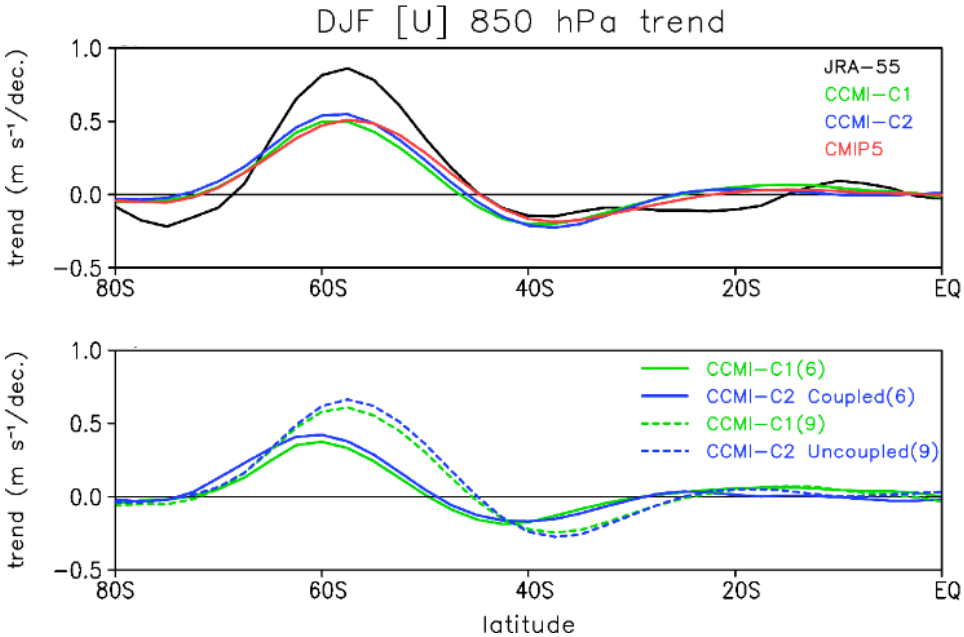

Figure 6. The 850 hPa zonal wind trends from JRA-55 and model output and sub-composite for the six models with a coupled ocean and the nine models where surface boundary conditions are prescribed (see table 1).

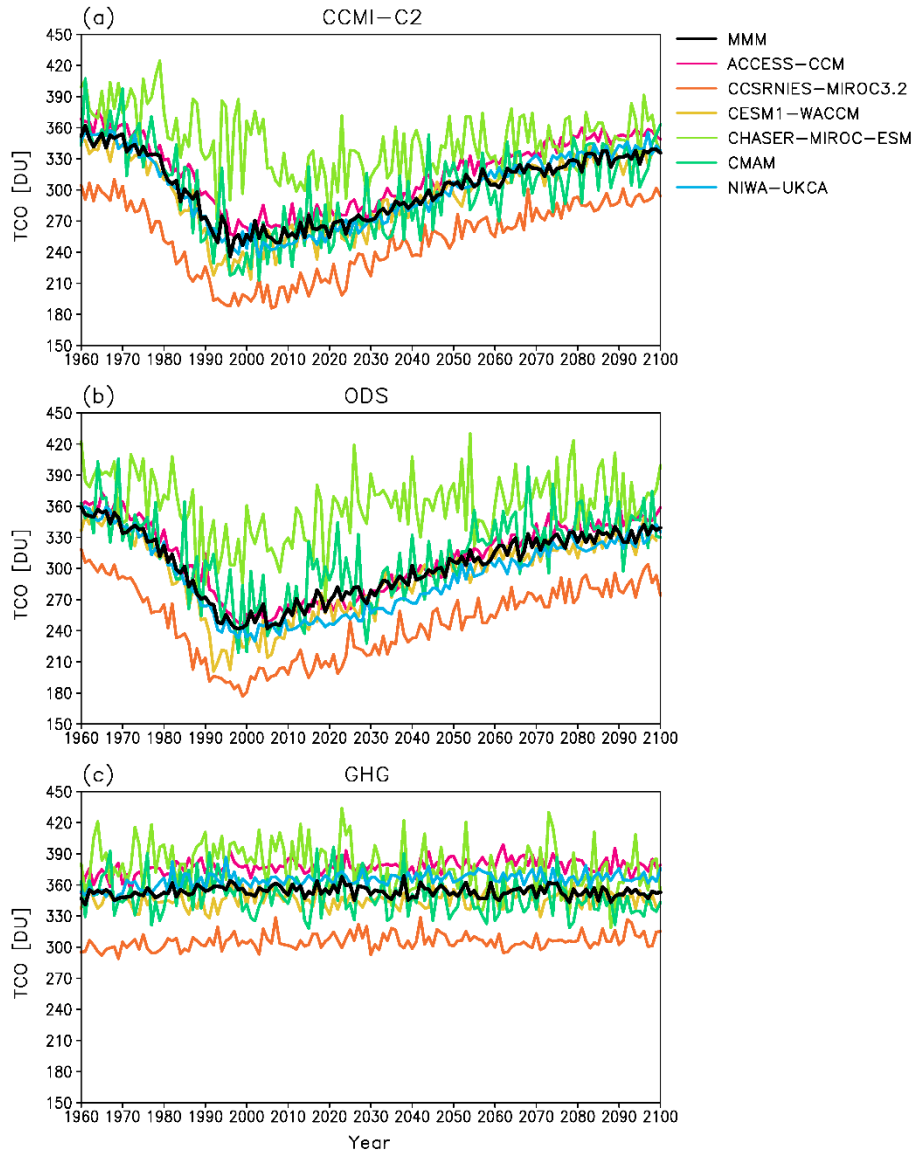

Figure 7. Temporal evolution of September-November (SON) total column ozone (TCO), integrated poleward of 60°S, from (a) CCMI-C2, (b) ODS and (c) GHG runs.

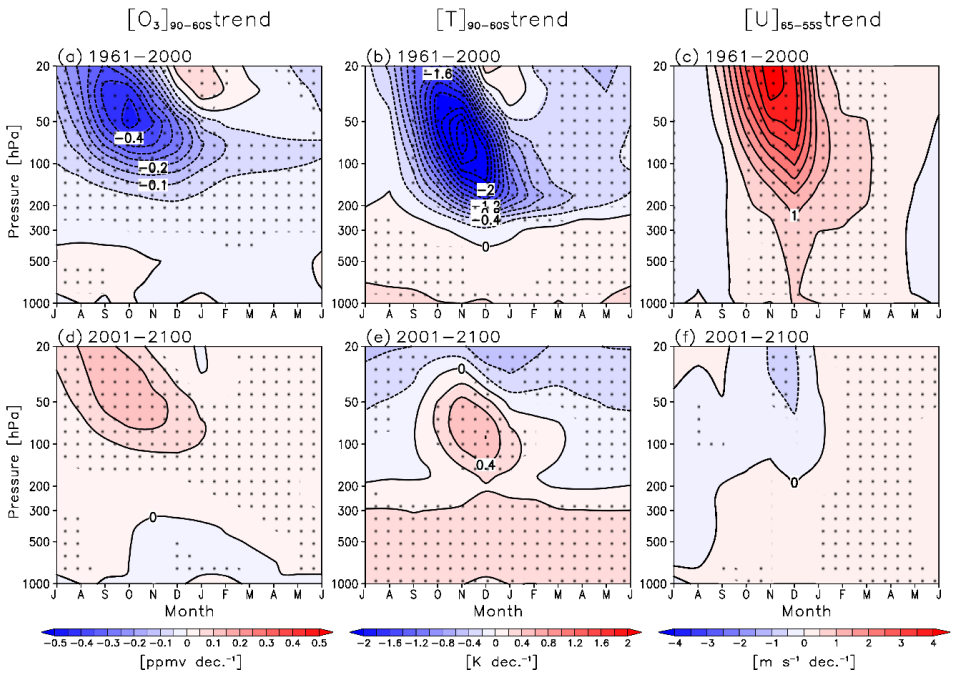

Figure 8. Multi-model mean (MMM) linear trends of the monthly mean polar (a) ozone [O3] and (b) temperature [T] averaged over 60°-90°S for the period of 1961-2000 in the CCMI-C2 runs. (c) Same as (a), but for the zonal wind [U] averaged over 55°-65°S. Starting month in the x-axis is July. Statistically significant trends are dotted at the 95% level. (d-f) Same as (a-c) but for the period of 2001-2100.

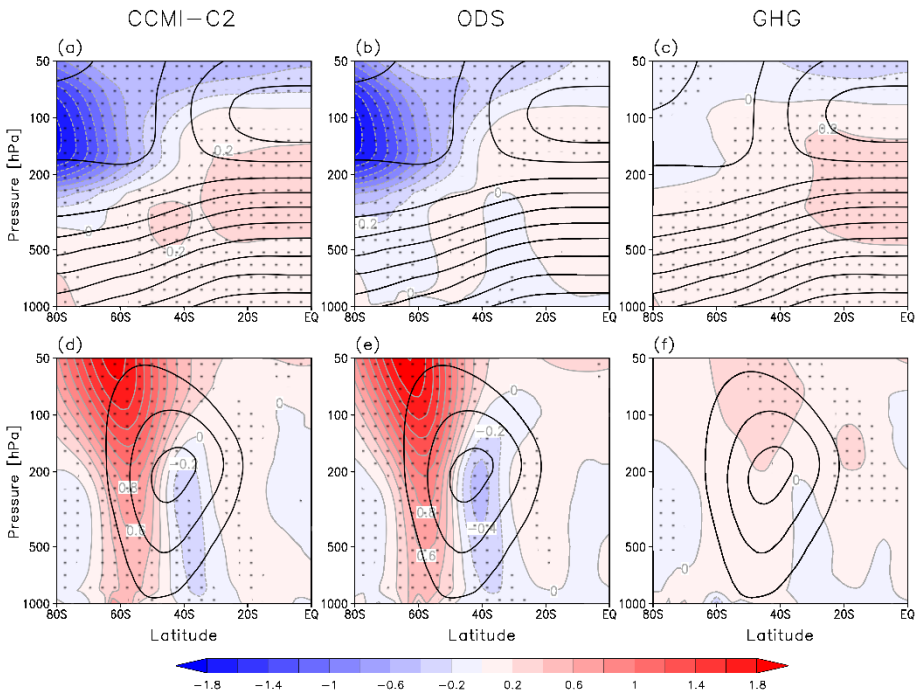

Figure 9. The MMM long-term mean (thick black contour) and linear trend (shading) of DJF temperature over the period of 1961-2000 for (a) CCMI-C2, (b) ODS, and (c) GHG runs. (d-f) Same as (a-c) but for the zonal wind. Contour intervals are 10 K starting from 200K (Figure 9a-9c) and 10 m s^{-1} starting from 10 m s^{-1} (Figure 9d-9f). Statistically significant trends are dotted at the 95% level.

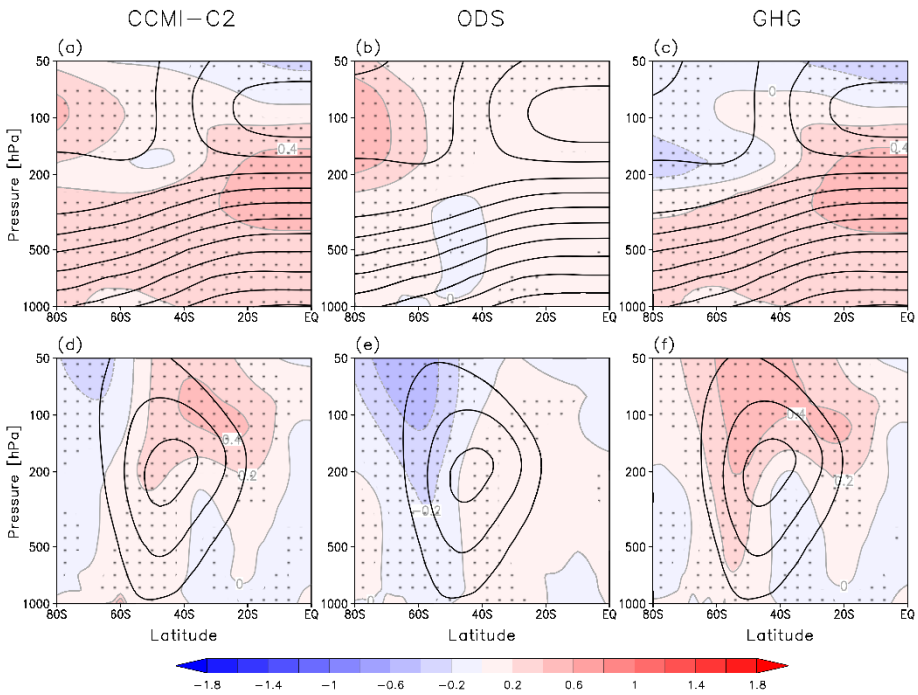

Figure 10. Same as Fig. 9 but for the period of 2001-2100.

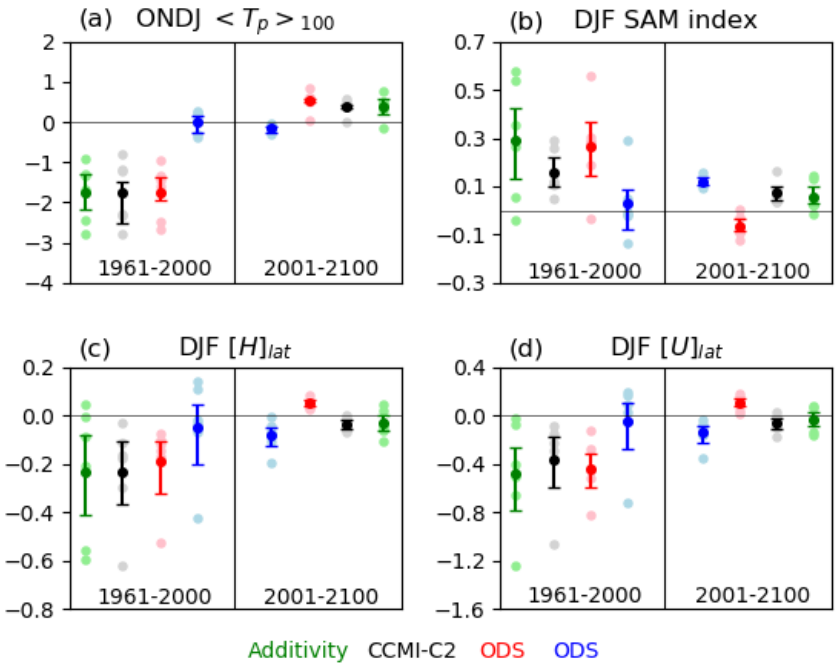

Figure 11. (a) The ONDJ polar temperature trend at 100 hPa (K /decade) for the period of (left) 1961-2000 and (right) 2001-2100. MMM trends are shown in closed circles with 5-95% confidence levels by a bootstrap method for the additivity (green), CCMI-C2 (black), ODS (red), and GHG (blue) runs. Each model trend is denoted with light colored circles. MMM values become statistically significant when the 5-95% confidence limits do not intersect the zero trend line. (b, c, and d) Same as (a) but for the trends in SAM index (decade^{-1}), Hadley cell edge (degree/decade), and DJF 850-hPa jet location (degree/decade), respectively.

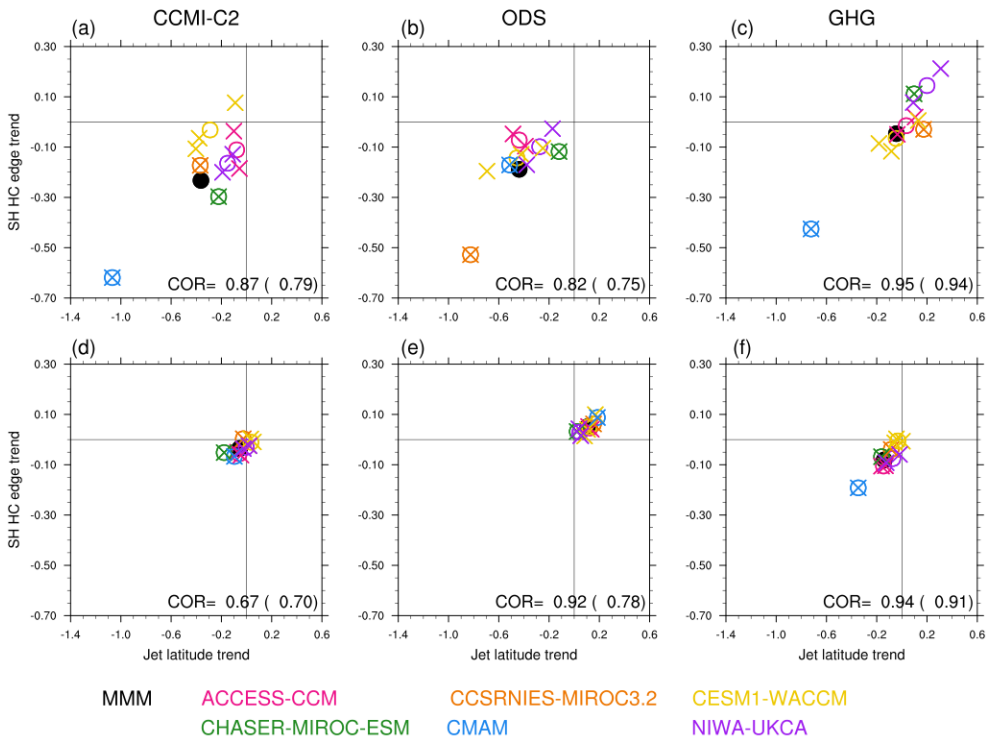

Figure 12. The relationship of DJF jet-latitude trends to DJF Hadley-cell edge trends over the period of 1961-2000 for (a) CCMI-C2, (b) ODS, and (c) GHG runs. (d-f) Same as (a-c) but for the period of 2001-2100. Each model ensemble mean is denoted with open circles. Each ensemble is denoted with a x mark. Correlation coefficient between the two variables is calculated for all model ensemble means and for all ensembles (shown in parenthesis).

초 록

CCMI 모형에서 성층권 오존의 변화가 남반구 순환 변화에 미치는 영향

한보름
협동과정 계산과학
석사과정
서울대학교

최신 대기화학 모형인 CCMI 모형을 사용하여 오존과 온실기체가 남반구 대기 대순환에 미치는 영향을 분석하였다. 대부분의 CCMI 모형은 과거 오존 전량과 남반구 동서평균 순환을 관측과 유사하게 모의하였다. 과거 남반구 순환의 변화는 모형의 경계조건과 오존의 접합방법에 민감하지 않았다. 온실기체도 남반구 순환을 바꿀 수 있다고 알려져 있기 때문에 온실기체와 오존감소물질을 1960 년대 수준으로 각각 고정한 실험을 통해서 두 인자간 상대적 중요성을 살펴보았다. 선행연구와 마찬가지로 과거에는 오존이 남반구 순환에 지배적인 영향을 미치고 온실가스의 영향은 모형마다 다르게 예측하여 모형별 불확실성이

컸다. 미래의 경우 오존이 회복하면서 과거와는 반대로 남반구 순환에 영향을 미치는 데 이때 온실가스의 영향과 상쇄되어 미래의 남반구 순환의 변화는 과거에 비해 그 강도가 약하게 변화하는 것을 확인 하였다. 또한 미래에는 오존과 온실가스가 비슷하게 남반구 대기 대순환에 중요한 영향을 미쳤다.

주요어: 성층권 오존, 온실기체, 남반구 순환, 제트 위치, 해들리 순환 팽창

학번: 2018-20597